

PACS numbers: 42.55.Rz; 42.60.Jf; 42.60.Lh; 81.05.Je; 81.05.Mh
DOI: 10.1070/QE2015v045n05ABEH015769

Re^{3+}:YAG laser ceramics: synthesis, optical properties and laser characteristics

S.N. Bagayev, V.V. Osipov, S.M. Vatnik, V.A. Shitov, I.Sh. Steinberg, I.A. Vedin, P.F. Kurbatov, K.E. Luk'yashin, R.N. Maksimov, V.I. Solomonov, P.E. Tverdokhleb

Abstract. **Highly transparent yttrium aluminium garnet ceramics doped with holmium or ytterbium or neodymium are synthesised. The ceramics were made of a mixture of nanopowders synthesised by laser ablation. The structural and spectral characteristics of ceramics are studied. In the samples with holmium Ho^{3+} and neodymium Nd^{3+} ions, lasing was achieved with a slope efficiency of 40% and 35.3%, respectively; the maximum laser power exceeded 4 W. The internal absorption and scattering losses for 1% Nd:YAG ceramics are estimated to be 1.6×10^{-2} cm^{-1}.**

Keywords: *yttrium aluminium garnet, holmium, ytterbium, neodymium, nanopowder, ceramics, transmission spectrum, lasing.*

1. Introduction

Highly transparent Nd:YAG laser ceramics was synthesised for the first time in 1995 by a group of Japanese scientists headed by Ikesue [1]; in specific laser power, this ceramics was comparable with single crystals. The highly transparent YAG-based ceramics turned out to be extremely attractive as a material for active laser elements, which is explained by a relatively simple production technology, low cost, unlimited dimensions and the possibility of creating multilayer structures. It was found that, to achieve a high transparency of ceramics, it is necessary to fulfil some essential requirements, which include a low thickness of intergrain boundaries (~1 nm) and the absence of pores and secondary phases (their concentration must be lower than 1–10 ppm) [2, 3].

In the course of investigations, we developed two ceramics synthesis methods satisfying these requirements. In the first method, which was described in detail in [2] and called the solid-phase reaction method [3] or the reaction sintering method [4], commercial oxide powders after long milling are mixed, compacted and sintered. In this case, the phase transformations of Nd_2O_3, Y_2O_3 and Al_2O_3 into $Nd^{3+}:Y_3Al_5O_{12}$ (Nd:YAG) occur during vacuum sintering of ceramics. In the second method [5, 6], ceramics is synthesised from Nd:YAG powders. Both methods have some modifications differing by the methods of production of nanopowders, their mixing, doping with bonding and sintering additives, methods of compaction of nanopowders and sintering regimes [1, 2, 7, 8]. Due to these technological features, ceramic samples with a theoretical transparency (~84%) have been synthesised only by a few scientific groups. One of the reasons for this is, in our opinion, insufficiently accurate maintenance of the stoichiometric composition of yttrium aluminium garnet.

Previously [9], we showed that the YAG stoichiometry can be achieved with a required accuracy by using a mixture of $Nd^{3+}:Y_2O_3$ and Al_2O_3 nanopowders. It is only necessary to accurately weight the components. Actually, our method of synthesis of highly transparent Nd:YAG ceramics is similar to the reaction sintering method with the only difference that Nd is already incorporated into the Y_2O_3 lattice. The aim of the present work is to study the possibility of using this method to synthesise highly transparent YAG ceramics doped with various rare-earth ions (Re = Nd, Yb, Ho) from a mixture of nanopowders ($Re^{3+}:Y_2O_3$ and Al_2O_3 produced by laser ablation) without surfactants but with the use of tetraethylorthosilicate (TEOS) as a sintering additive.

2. Objects of study

Coarse commercial powders Ho_2O_3, Yb_2O_3, Nd_2O_3, Y_2O_3 and Al_2O_3 with a purity grade at least 99.99% were used to made laser targets of four compositions ($Ho^{3+}:Y_2O_3$, $Yb^{3+}:Y_2O_3$, $Nd^{3+}:Y_2O_3$ and Al_2O_3), which were than evaporated by radiation of a CO_2 laser. The concentration of Ho, Yb and Nd rare-earth ions in the first three compositions was about 1 at%. Nanoparticles with an average size of 12–15 nm were formed upon vapour condensation in an air flow. The technology of laser synthesis of oxide nanopowders is described in more detail in [9].

Next, $Re^{3+}:Y_2O_3$ and Al_2O_3 nanopowders in the proportion $(Re + Y)_2O_3:Al_2O_3 = 3:5$ were stirred during 48 h in ethanol with zirconium oxide balls. At the stirring stage, we used TEOS in amount of 0.5 wt% as a sintering additive. The mass ratio of nanopowder, balls and ethanol was 1:4:8. Then, the mixture was evaporated in a vacuum rotary evaporator and annealed in air at a temperature of 600 °C for three hours to remove organic impurities. During this process, no agglomeration of nanopowders was observed.

The dry annealed mixture of nanopowders was compacted into pellets with a relative density of 20%, which were then annealed in an atmospheric furnace at a temperature of 1200 °C for three hours. Then, these pellets were milled in

S.N. Bagayev, S.M. Vatnik, I.A. Vedin, P.F. Kurbatov Institute of Laser Physics, Siberian Branch, Russian Academy of Sciences, prosp. Akad. Lavrent'eva 13/3, 630090 Novosibirsk, Russia; e-mail: vatnik@laser.nsc.ru;
V.V. Osipov, V.A. Shitov, K.E. Luk'yashin, R.N. Maksimov, V.I. Solomonov Institute of Electrophysics, Ural Branch, Russian Academy of Sciences, ul. Amundsena 106, 620016 Ekaterinburg, Russia; e-mail: osipov@iep.uran.ru, vlad@iep.uran.ru;
I.Sh. Steinberg, P.E. Tverdokhleb Institute of Automation and Electrometry, Siberian Branch, Russian Academy of Sciences, prosp. Akad. Koptyuga 1, 630090 Novosibirsk, Russia

Received 29 January 2015; revision received 6 February 2015
Kvantovaya Elektronika **45** (5) 492–497 (2015)
Translated by M.N. Basieva

ethanol by yttria-stabilised zirconia (YSZ) balls during 48 h, after which the mixtures were evaporated and dried.

The obtained products were compacted into disks 15 mm in diameter and 2–4 mm thick by dry uniaxial static pressing under a pressure of 200 MPa. The density of Re:YAG compacts was ~50% of the X-ray density of this material. Then, the compacts were sintered in a vacuum furnace at a temperature of 1780 °C for 20 h. After this, the ceramic samples were bleached by annealing and mechanically polished. According to the X-ray diffraction analysis performed using a D8 Discover diffractometer, the main crystal structure of ceramic samples corresponded to yttrium aluminium garnet. Additionally, we analysed the existence of secondary phases by the luminescent method [10], which allows one to detect the presence of secondary phases with a concentration below 1%. If secondary phases were detected, the proportion of nanopowders was corrected. As a result, we produced ceramic samples in the form of nearly perfect polycrystals.

3. Results and discussion

Figure 1 shows a photograph of sintered Re:YAG ceramic samples after bleaching and polishing.

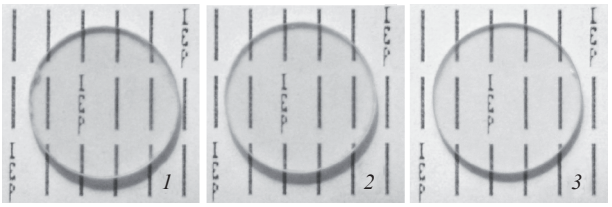

Figure 1. Photographs of (*1*) Ho:YAG, (*2*) Yb:YAG and (*3*) Nd:YAG ceramics.

Structural characteristics. Using an OLYMPUS BX51TRF-5 optical microscope, we estimated the average size of crystallites to be 14, 15 and 17 μm in the samples of Ho:YAG, Yb:YAG and Nd:YAG ceramics, respectively; the fraction of scattering centres in these samples did not exceed 30 ppm.

To study the depth distribution of inhomogeneities in optical ceramics, we used the method of collinear heterodyne detection (Fig. 2), which uses two coherent focused light beams – reference beam (*1*) and heterodyne beam (*2*). The heterodyne beam frequency is shifted by $\Delta F = 88$ MHz with respect to the reference beam frequency. In the region of intersection of these focused beams, a moving interference micrograting is formed, which overlaps with a noise grating (*4*) inside the laser ceramic sample (*3*). The light beam (*5*) is formed as a result of diffraction of the heterodyne beam (*2*) on the noise grating. If the spatial frequency of the noise grating is equal or close to the spatial frequency of the moving micrograting, then the light beam (*5*) will propagate in the same direction (collinearly) as the reference beam (*1*). The interaction of two collinear beams with different frequencies leads to the appearance of a photocurrent with a difference frequency ΔF at the exit of a photodiode (*6*). This signal carries information on the noise grating amplitude.

As a radiation source, we used a semiconductor laser emitting at a wavelength of 660 nm, while a microobjective with a working distance of 2 mm and a numerical aperture

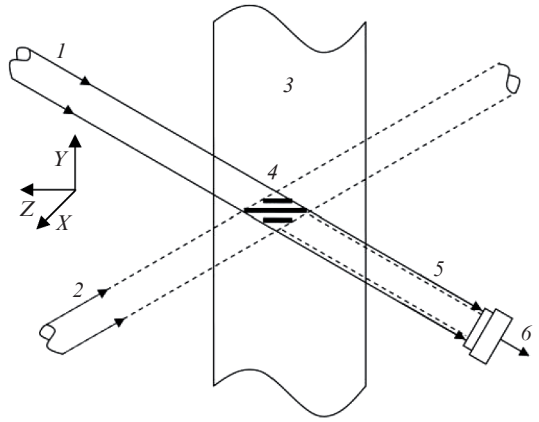

Figure 2. Scheme for investigating the spatial distribution of optical inhomogeneity in a bulk material using collinear heterodyne detection.

NA = 0.6 was used as a focusing objective. In the focal plane of the microobjective, a micrograting with dimensions $\Delta x \times \Delta y = 0.8 \times 1.3$ μm was formed. The micrograting size (at half maximum) along the sample thickness for diffraction-limited beams was $\Delta z = 6.8$ μm. It should be noted that the heterodyne detection occurs only in the region of intersection of beams (*1*) and (*2*), where the micrograting forms. A detailed description of the method is given in [11].

Moving the sample along the Z axis (in depth), one can record a one-dimensional distribution of optical inhomogeneities. However, more comprehensive information about the inhomogeneity distribution is provided by a two-dimensional pattern obtained as a result of series of in-depth scans with sequential shifts in the transverse direction (along the Y axis). In particular, Fig. 3a shows an example of a synthetic image of distribution of optical inhomogeneities (topograph), which is obtained by this two-dimensional scanning of Ho:YAG ceramics. From Fig. 3, one can see that the number of inhomogeneities in ceramics, at least in this scanning range, is

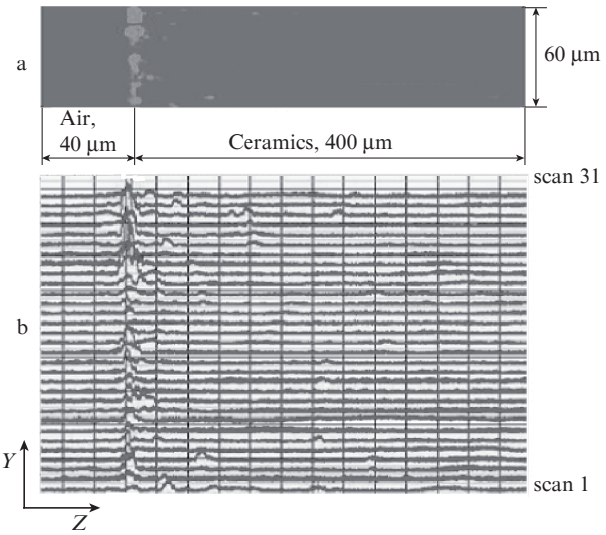

Figure 3. Graphical representation of a two-dimensional scan of Ho:YAG ceramics: (a) topograph of the region $Y \times Z = 60 \times 400$ μm and (b) amplitudes of reading signals in all the reading cycles (from the first to the thirty first).

small and their size does not exceed 1–2 μm since they are not seen in neighbouring scans. On the assumption of a phase character of inhomogeneities, the change in the refractive index due their presence is $\sim 10^{-4}$.

Figure 4 presents the results of similar investigations of Nd:YAG sample No. 1570 (neodymium concentration 1 at %). One can see that the scattering noise in the volume of this sample is rather low. As an example, let us analyse scan 1 (Fig. 4b) in more detail. Since the heterodyne detection provides information not only about the signal amplitude but also about the signal phase, in Fig. 5 we present the photodetector signal amplitude and phase distributions obtained by scanning.

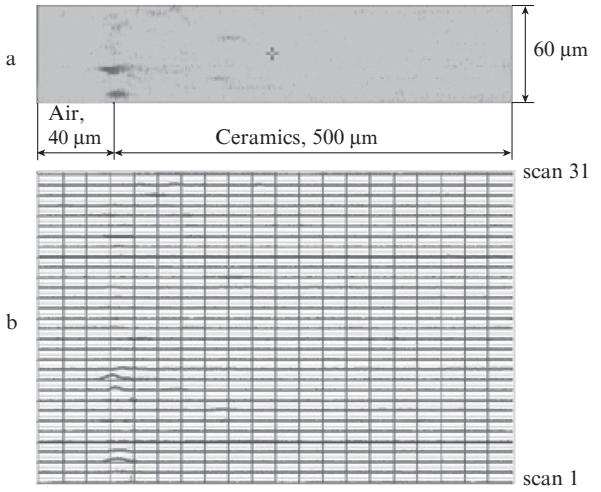

Figure 4. Graphical representation of a two-dimensional scan of Nd:YAG laser ceramics: (a) topograph of the region $Y \times Z = 60 \times 500$ μm and (b) amplitudes of reading signals in all (31) scanning cycles.

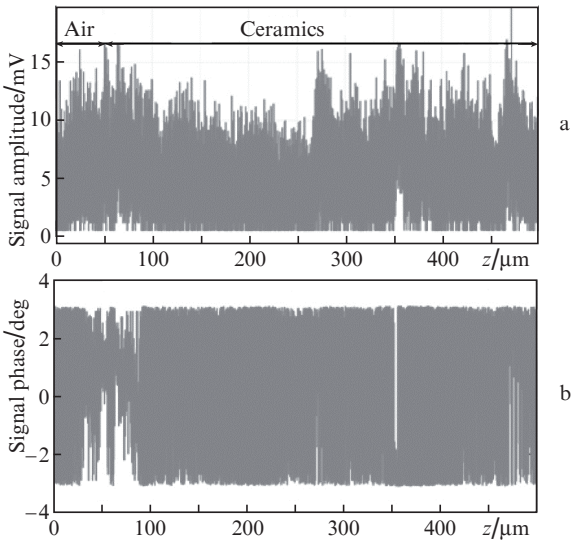

Figure 5. (a) Reading signal amplitude and (b) phase distributions obtained by depth scanning of Nd:YAG ceramics (scan 1 in Fig. 4b).

The root-mean-square noise in air is 5 mV and is determined by the noise of the photocurrent amplifier and of the components of electronic schemes. The root-mean-square noise voltage in ceramics (50–540 μm) is 6.4 mV and only slightly exceeds the scattering noise in air. The reading signal amplitude distribution in this case does not allow one to separate the information about scattering centres in the scanning region. At the same time, the phase distribution pattern is more informative. In the regions with a weak scattering, the phase is randomly distributed from $-\pi$ to π, but slightly changes in the presence of a scattering centre. In particular, the phase distribution shown in Fig. 5b allows one to easily detect the ceramics boundary (range from 40 to 60 μm), as well as small scattering centres lying along the scanning line at depths of 270, 360 and 470 μm. The size of the region of a weakly changing phase near 360 μm is 6–7 μm, which corresponds to the depth point spread function. Therefore, we can conclude that the inhomogeneity size does not exceed 1 μm. More precise data on the inhomogeneity size can be obtained having a priori information about its nature.

Spectral characteristics. Figure 6 presents the transmission spectra of all the three ceramic compositions. The spectra were recorded on a Shimadzu UV-1700 spectrophotometer within the range 200–1100 nm at room temperature. One can see that the transmission of Nd:YAG ceramics near a wavelength of 1 μm reaches almost the limiting value (~84%) achieved in the best laser single crystals.

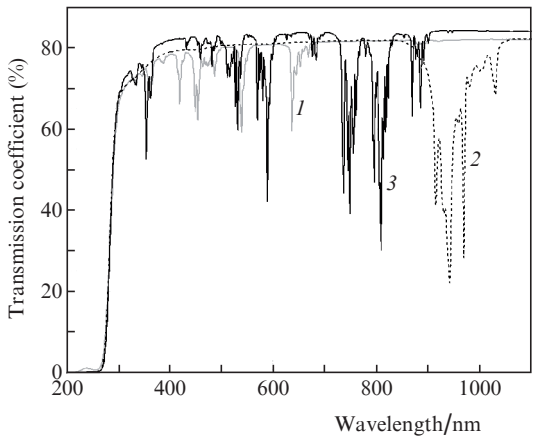

Figure 6. Transmission spectra of (*1*) Ho:YAG, (*2*) Yb:YAG and (*3*) Nd:YAG ceramics.

Laser characteristics. We studied the lasing properties of Ho:YAG and Nd:YAG ceramics. The first ceramics was chosen due to the fact that the trivalent holmium ion emits in the range 0.8–2.1 μm. Lasers operating within this wavelength range are of great interest for a number of applications, including remote probing of the atmosphere [12, 13], range finding [14], ecological monitoring [15, 16] and pumping of optical parametric oscillators [17–19]. The use of highly transparent laser ceramics as active elements considerably extends the capabilities of these laser systems due to, first of all, an increase in the specific energy output and in the lasing efficiency [20, 21]. The lasing characteristics of Ho:YAG ceramics were studied in [22–24]. Upon pumping into the absorption maximum at a wavelength of 1.907 μm, the output laser power exceeded 20 W and the slope efficiency η was higher that 60%, which closely approaches the corresponding parameters for crystalline active elements [19, 25]. The choice of Nd:YAG ceramics is explained by the fact that it is most promising for creating high-power lasers [2, 5, 6]. In both

cases, we used ceramic samples in the form of disks with dimensions ∅11 × 1 mm.

Ho:YAG ceramics. The ceramics was pumped by a disk thulium laser with a wavelength of 1.85 μm (potassium lutetium double tungstate crystal 5% Tm:KLuW 250 μm thick). Since the optical density of ceramics is comparatively low (about 15%) even in the absorption maximum at λ = 1.907 μm, the ceramic sample was pumped using an intracavity scheme. In our case, the cavity was formed by a highly reflecting mirror deposited on the surface of the 5% Tm:KLuW crystal and a partially transmitting mirror (T_{oc} = 0.6%) on the output surface of the ceramic sample. All optical surfaces inside the cavity were antireflection coated for the spectral range 1.85–2.1 μm with residual losses for each coating no higher than 0.1% in the region of 1.85 μm and ~0.5% in the region of 2.1 μm. The thulium laser beam was focused on the ceramic sample by a fused quartz (KI) lens with a focal distance of 18 mm, which was placed at identical distances from the sample and the thulium laser disk. The physical cavity length was 50 mm. The 5% Tm:KLuW active disk was pumped by collimated beams of two laser diode arrays (λ_{ex} = 806 nm); the pump spot diameter was 0.95 mm. To reduce heat flows, all measurements were performed in a quasi-cw regime with an off-duty ratio of 14%, 7-ms current pulses of the arrays, and a repetition period of 50 ms. In all the cases, the absorbed pump power was determined as a difference between the optical powers of the incident and output light beams (pump and laser powers) and recorded by an Ophir L30A power meter. The laser spectra were measured using an MDR-204 monochromator, an FR-185 photoresistor and a Unipan-233 selective nanovoltmeter; the spectral resolution (FWHM) was ~0.5 nm.

The dependences of the overage output laser power on the average absorbed pump power are shown in Fig. 7. Curve (*2*) is plotted for a Ho:YAG ceramic sample with dielectric coatings and corresponds to the total output power of the thulium laser (λ = 1.85 μm) and the ceramic sample (λ = 2.09 μm). Curve (*1*) corresponds to the output power of the thulium laser at λ = 1.85 μm with replacement of the ceramic sample by a plane dielectric mirror with a transmission of 0.6%, while curves (*3*) and (*4*) correspond to the powers at wavelengths of 1.85 and 2.09 μm and are calculated from relative intensities of laser spectra.

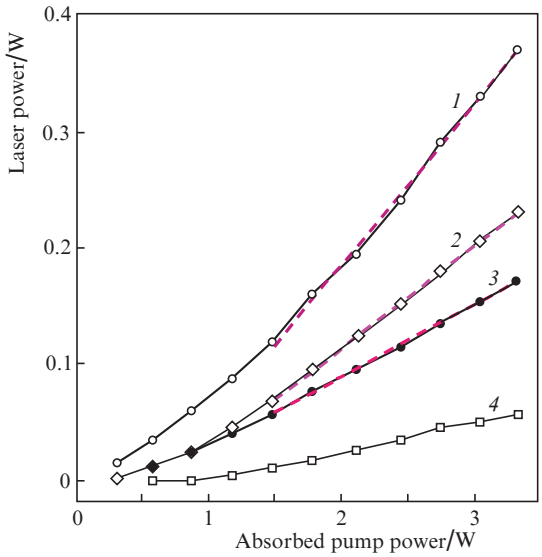

Figure 7. Dependences of the average output laser power on the absorbed pump power. Dashed curves show the linear approximations of the corresponding dependences used to determine the slope efficiencies η_{exp}.

Beginning from the threshold pump power of ~1.0 W (see Fig. 7), two light fields corresponding to the $^3F_4 \rightarrow {}^3H_6$ transitions of Tm^{3+} ions in the KLuW matrix (λ = 1.85 μm) and the $^5I_7 \rightarrow {}^5I_8$ transition of Ho^{3+} ions in the YAG matrix (λ = 2.09 μm) are simultaneously excited in the cavity. The absorption of Ho:YAG ceramics (per two passes) at λ = 1.85 μm (T_{abs}) was 3% in the unsaturated absorption regime and 2.4% in the lasing regime with allowance for 20% inversion [24]. Thus, the total losses in the cavity with Ho:YAG ceramics were determined as $T_{abs} + T_{oc} + T_{loss}$ (where T_{loss} are the parasitic absorption and scattering losses in the cavity per round-trip) at the wavelength 1.85 μm. In the case of replacement of ceramics by an output mirror with a transmission T_{oc}, absorption was absent (T_{abs} = 0). In accordance with the general relations [26], the experimentally determined slope efficiency can be written as

$$\eta_{exp} = \eta T_{oc}/(T_{abs} + T_{oc} + T_{loss}), \quad (1)$$

where η is the maximum slope efficiency for an ideal lossless cavity. Applying (1) to the dependences described by curves (*1*) and (*3*), we obtain the relation

$$(0.6\% + T_{loss})/(3.0\% + T_{loss}) = (6.2\%)/(14.0\%) = 0.44, \quad (2)$$

where 14.0% and 6.2% are the slope efficiencies for curves (*1*) and (*3*). Thus, relations (1) and (2) allow one to estimate the losses T_{loss} to be ~1.2% at η = 45%, which well agrees with the results of works [27, 28]. The estimate $T_{loss} \approx 1.2\%$ seems quite likely due to a large number of optical surfaces inside the cavity. According to these estimates, the light power absorbed by ceramics fivefold exceeds the output laser power with respect to curve (*3*) (see Fig. 7).

On the other hand, losses in the cavity at a wavelength of 2.09 μm increase at least to $T_{loss}(2.09) \approx 3.0\%$ first of all due to an increase in the residual reflection from the lens surfaces, i.e., the intracavity losses are at least five times higher than the transmission coefficient of the output mirror $T_{oc}(2.09)$ equal to 0.6%. Thus, comparing curves (*3*) and (*4*) with allowance for (1), we can estimate the limiting slope efficiency of Ho:YAG ceramics at the $^5I_7 \rightarrow {}^5I_8$ transition in the case of intracavity pumping with respect to the absorbed power at a wavelength of 1.85 μm to be $\eta \approx 40\%$. This is approximately twice as low as the corresponding parameter for Ho:YAG crystals [18, 24], which can be explained by the existence of structural microdefects in the ceramics.

Nd:YAG ceramics. Laser characteristics of 1% Nd:YAG ceramics were studied in sample No. 1570 synthesised at the Institute of Electrophysics, Ural Branch, Russian Academy of Sciences, and in reference sample R10097 synthesised at Baikowski Ltd. (Konoshima Chem.). The samples had shapes of disks with plane polished surfaces and dimensions of ∅11 × 1.5 mm and ∅10 × 2.2 mm, respectively. For comparison, the transmission coefficients of both samples were additionally measured on a Shimadzu UV-3101PC spectrophotometer within the spectral range 800–1100 nm (Fig. 8).

In both samples, the absorption maxima in the near IR region are centred at a wavelength of 808 nm. It is important to note that the transmission of both ceramics in the transpar-

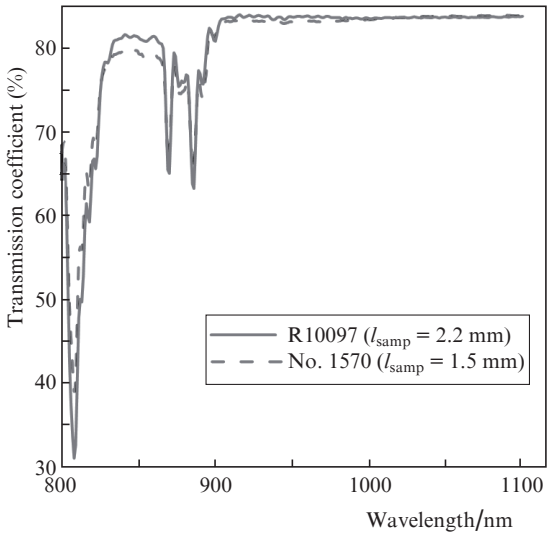

Figure 8. Transmission spectra of 1% Nd:YAG ceramic samples R10097 (solid curve) and No. 1570 (dashed curve).

ency range (1000–1100 nm) is the same within the measurement error (±0.5%, which is determined by the long-term stability of the spectrophotometer) and corresponds to the calculated transmission T_c = 83.9% of an optical material with the refractive index n = 1.815 (the case of ideal homogeneous ceramics with allowance for only the Fresnel reflection losses).

Then, the surfaces of disks were coated with dielectric layers, namely, a broadband antireflection coating with the residual reflection $R < 0.15\%$ at the pump (808 nm) and laser (1064 nm) wavelengths was deposited on one of the surfaces, and a combined reflecting coating consisting of a highly reflecting dielectric mirror ($R > 99.8\%$ at λ = 1064 and 808 nm) and an additional metallisation layer, which decreased the residual transmission losses to ~0.05% for both wavelengths, was deposited on the other surface. For effective heat removal, the ceramic disks were mounted on copper heat sinks with an intermediate indium foil layer 100 μm thick using different soldering and pressing methods.

Pumping of 1% Nd:YAG samples Nos 1570 and R10097 was performed by two diode arrays, whose beams were focused by two-mirror collimators and auxiliary optics into a round spot 1.2 mm in diameter in the focus. The total optical pump power reached 50 W; the radiation of arrays had a spectral width of ~4 nm and was centred at a wavelength of 808 nm due to appropriate thermal stabilisation of array housings.

In the course of preliminary studies of lasing characteristics of samples, it was found that a change in the physical cavity length L within the range 20–100 mm only slightly (within ~5%) affects the output laser power, while at $L > 100$ mm the power begins to rapidly decrease because the cavity leaves the stability region. Therefore, all laser experiments were performed at L = 20 mm, at which the output laser power was maximum (L = 20 mm is the minimal length at which the pump beam is not blocked by the output mirror). As output mirrors, we used two spherical concave mirrors with the curvature radius r = 100 mm and the transmission coefficients T = 2.6% and 10.5% at λ = 1064 nm. The Gaussian beam diameter for a cavity with these parameters was 0.23 mm. Since the pump spot diameter was considerably larger (1.2 mm), we compared the maximum output power and laser efficiency of laser ceramics ignoring the mode composition of radiation. The optical pump and laser powers were measured with an Ophir L30A power meter.

Figure 9 shows the measured laser characteristics of 1% Nd:YAG ceramic samples No. 1570 and R10097 for a two-pass pumpng scheme; the absorbed power was calculated as a difference between the incident and output powers. According to the presented results, the lasing thresholds of both samples almost coincide, the slope efficiencies being 41.1% (T = 2.6%) and 43.6% (T = 10.5%) for sample R10097, as well as 29.8% (T = 2.6%) and 35.5% (T = 10.5%) for sample No. 1570. Comparing the slope efficiencies at different transmissions of the output mirror, we can estimate the intracavity losses (per two passes) to be 0.2% for R10097 ceramics and 0.7% for ceramic sample No. 1570. Assuming that the absorption and scattering losses in the volume of the reference sample R10097 are considerably lower than the losses at optical surfaces (antireflection coatings and mirrors, including the output one), we find that the losses in the studied sample No. 1570 are ~0.5% at the laser wavelength (two passes), i.e., the specific losses are $\sim 1.6 \times 10^{-2}$ cm^{-1}. At these losses, the slope efficiency of ceramic sample No. 1570 (35.5%) reaches 80% of the corresponding parameter for the reference sample R10097 (43.6%).

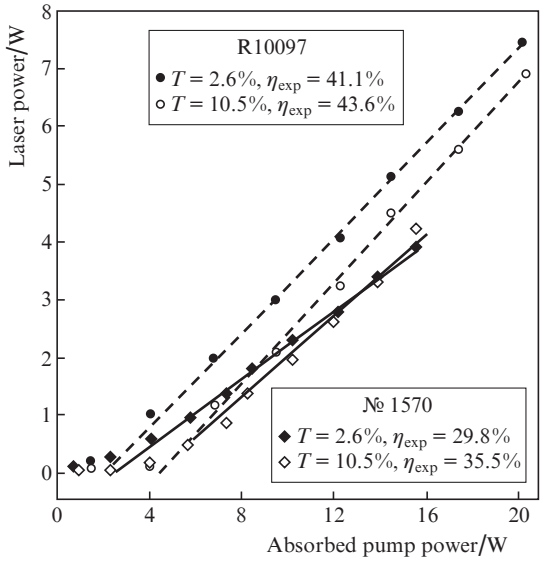

Figure 9. Dependences of the output laser power on the absorbed pump power for 1% Nd:YAG laser ceramic samples No. 1570 (rhombs) and R10097 (circles).

4. Conclusions

In this work, we described the technology of synthesis of highly transparent ceramics based on yttrium aluminium garnet doped with holmium, ytterbium and neodymium ions. Ceramic samples with a transparency close to theoretical transmission are synthesised. The lasing thresholds and slope efficiencies of Ho:YAG and Nd:YAG ceramics are close to the corresponding parameters of the best foreign samples. However, the achieved slope efficiencies of 40% (Ho:YAG) and 36% (Nd:YAG) are lower than the world's best values.

This can be related to a decrease in the transparency in the short-wavelength spectral region due to, most probably, the presence of small inhomogeneities. In this connection, further improvement of the optical homogeneity of laser ceramics remains a topical scientific and technical problem, which is of high priority for the development of modern multikilowatt solid-state laser systems.

Acknowledgements. This work was supported by the Presidium of the Russian Academy of Sciences (Extreme Light Fields and Their Applications Programme) and by the Russian Foundation for Basic Research (Grant Nos 14-08-00181 and 14-02-00732-a).

References

1. Ikesue A., Kinoshita T., Kamata K., Yoshida K. *J. Am. Ceram. Soc*., **78**, 1033 (1995).
2. Ikesue A., Aung Y.L., Taira T., Kamimura T., Yoshida K., Messing G.L. *Annu. Rev. Mater. Res*., **36**, 397 (2006).
3. Kochawattana S., Stevenson A., Lee S.-H., Ramirez M., Gopalan V., Dumm J., Castillo V.K., Quarles G.J., Messing G.L. *J. Eur. Ceram. Soc*., **28**, 1527 (2008).
4. Byer R.L. *Proc. 3rd Laser Ceramics Symposium: International Symposium on Transparent Ceramics for Photonic Applications* (Paris, CNRS, 2007, IO-G-1).
5. Lu J., Ueda K., Yagi H., Yanagitani T., Akiyama Y., Kaminskii A.A. *J. Alloy. Compd*., **341**, 220 (2002).
6. Lu J., Yagi H., Takaichi K., Uematsu T., Bison J.-F., Feng Y., Shirakawa A., Ueda K.-I., Yanagitani T., Kaminskii A.A. *Appl. Phys. B*, **79**, 25 (2004).
7. Bakunov V.S., Belyakov A.V., Lukin E.S., Shayakhmetov U.Sh. *Oksidnaya keramika: spekanie i polzuchest'* (Oxide Ceramics: Sintering and Plastic Deformation) (Moscow: RKhTU im. D.I. Mendeleeva, 2007).
8. Bagayev S.N., Osipov V.V., Solomonov V.I., Shitov V.A, Maksimov R.N., Lukyashin K.E., Vatnik S.M., Vedin I.A. *Opt. Mater*., **34**, 1482 (2012).
9. Osipov V.V., Kotov Yu.A., Ivanov M.G., Samatov O.M., Lisenkov V.V., Platonov V.V., Murzakaev A.M., Medvedev A.I., Azarkevich E.I. *Laser Phys*., **16**, 116 (2006).
10. Osipov V.V., Solomonov V.I., Spirina A.V. *Opt. Zh*., **78** (6), 81 (2011).
11. Tverdokhleb P.E., Shchepetkin Yu.A., Shteinberg I.Sh., Vatnik S.M., Belikov A.Yu., Vedin I.A., Kurbatov P.F. *Kvantovaya Elektron*., **44** (6), 588 (2014) [*Quantum Electron*., **44** (6), 588 (2014)].
12. Fischer C., Sorokin E., Sorokina I.T., Sigrist M.W. *Opt. Lasers Eng*., **43**, 573 (2005).
13. Wang L., Gao C., Gao M., Li Y., Yue F., Liu L. *Opt. Eng*., **53**, 061603 (2013).
14. Mizutani K., Itabe T., Ishii Sh., Aoki T., Asai K., Sato A., Fukuoka H., Ishikawa T. *Proc. SPIE Int. Opt. Soc. Eng*., **7153**, 71530J (2008).
15. Godart A. *Physique,* **8**, 1100 (2007).
16. Gibert F., Flamant P.H., Bruneau D., Loth C. *Appl. Opt*., **45**, 4448 (2006).
17. Budni P.A., Pomeranz L.A., Lemons M.L., Miller C.A., Mosto J.R., Chicklis E.P. *J. Opt. Soc. Am. B*, **17**, 723 (2000).
18. Lippert E., Fonnum H., Arisholm G., Stenersen K. *Opt. Express*, **18**, 26475 (2010).
19. Haakestad M.W., Fonnum H., Arisholm G., Lippert E., Stenersen K. *Opt. Express*, **18**, 25379 (2010).
20. Qi Y., Zhu X., Lou Q., Ji J., Dong J., Wei R. *Opt. Express*, **13**, 8725 (2005).
21. Taira T. *IEEE J. Sel. Top. Quantum Electron*., **13**, 798 (2007).
22. Cheng X.J., Xu J.Q., Wang M.J., Jiang B.X., Zhang W.X., Pan Y.B. *Laser Phys. Lett*., **7**, 351 (2010).
23. Yang H., Zhang J., Qin X., Luo D., Ma J., Tang D., Chen H., Shen D., Zhang Q. *J. Am. Ceram. Soc*., **95**, 52 (2012).
24. Wang L., Gao C., Gao M., Li Y., Yue F., Zhang J., Tang D. *Opt. Express*, **22**, 254 (2014).
25. Lippert E., Nicolas S., Arisholm G., Stenersen K., Rustad G. *Appl. Opt*., **45**, 3839 (2006).
26. Svelto O. *Prinsiples of Lasers* (Heidelberg: Springer, 2010).
27. Vatnik S.M., Vedin I.A., Pujol M.-C., Mateos X., Carvajal J.J., Aguiló M., Díaz F., Griebner U., Petrov V. *Laser Phys. Lett*., **7**, 435 (2010).
28. Vatnik S.M., Vedin I.A., Segura M., Mateos X. *Opt. Lett*., **37**, 356 (2012).